THE ASTROPHYSICAL JOURNAL, 426:373–381, 1994 May 1

THE CORONAL ELECTRON DENSITY DISTRIBUTION DETERMINED FROM DUAL-FREQUENCY RANGING MEASUREMENTS DURING THE 1991 SOLAR CONJUNCTION OF THE *ULYSSES* SPACECRAFT

M. K. BIRD AND H. VOLLAND
Radioastronomisches Institut, Universität Bonn, Auf dem Hügel 71, 53121 Bonn, Germany
M. PÄTZOLD
Institut für Geophysik und Meterologie, Universität Köln, 50923 Köln, Germany
P. EDENHOFER
Institut für Hochfrequenztechnik, Ruhr-Universität Bochum, 44780 Bochum, Germany
AND
S. W. ASMAR AND J. P. BRENKLE
Jet Propulsion Laboratory, California Institute of Technology, 4800 Oak Grove Drive, Pasadena, CA 91109
Received 1992 November 23; accepted 1993 November 4

ABSTRACT

Dual-frequency ranging and Doppler measurements were conducted in support of the *Ulysses* Solar Corona Experiment at and around the spacecraft's first solar conjunction in 1991 August. The differential group delay time between range codes on the two downlink carrier signals at the wavelengths 13.1 and 3.6 cm, a direct measure of the total electron content between spacecraft and ground station, was used to derive the electron density distribution in the solar corona. Linear power-law representations of the coronal electron density were derived for the range of solar distances from 4 $R_\odot$ to 40 $R_\odot$ on both sides of the Sun. The corona was found to be very nearly symmetric; the radial falloff exponent being 2.54 ± 0.05 for occultation ingress (east solar limb) and 2.42 ± 0.05 for egress (west limb), respectively. The departure of these exponents from the inverse square relation implies that significant solar wind acceleration is occurring within the radial range of the observations. The electron density level was found to be considerably lower than that observed during the 1988 December solar occultation of *Voyager 2*. Although the smoothed sunspot number R_Z (a standard indicator of solar activity) was almost the same in 1988 December and 1991 August, the mean electron density at 20 $R_\odot$ was found to be $1.7 \pm 0.1 \times 10^3$ cm^{-3} during the *Ulysses* conjunction, a decline by almost a factor of 4 from the value obtained during the *Voyager* conjunction.

Subject headings: interplanetary medium — solar wind — Sun: corona — Sun: radio radiation

1. INTRODUCTION

The *Ulysses* Solar Corona Experiment (SCE), which uses the spacecraft's dual-frequency downlinks for radio-sounding observations of the interplanetary plasma near the Sun, was performed during the first solar conjunction (C_1) from 1991 May to September. Differential range observations with the two downlink carrier signals were used to derive the radial distribution of plasma in the solar corona and inner heliosphere. *Ulysses*, with its most favorable coronal-sounding opportunity during the in-ecliptic phase of the mission en route to its Jupiter encounter, was only the third spacecraft used to perform a dual-frequency ranging experiment during a solar occultation. Some preliminary results of these measurements were reported by Pätzold et al. (1992). A detailed description of the SCE investigation may be found in Bird et al. (1992).

The concept of determining the columnar electron density between a spacecraft and a tracking station on Earth with group time-delay measurements was known prior to the advent of interplanetary spacecraft (Kelso 1959). The first such measurements in interplanetary space were recorded as part of a uplink radio propagation experiment at the frequencies 50 and 425 MHz using *Pioneer 6* (Eshleman et al. 1966). Most of the interplanetary radio-sounding observations since these initial tests have been performed not with dedicated on-board instrumentation, but rather as a cost-effective extension of the spacecraft's range of exploration generally referred to as "radio science." The necessary radio telecommunications links between spacecraft and ground are utilized to probe intervening media along the signal ray path. Most prominent of these media are the atmospheres, ionospheres, rings, and tori of solar system objects. The one medium readily assessible to this technique is the global distribution of plasma in interplanetary space, particularly the inner heliosphere and solar corona during times of spacecraft superior conjunction.

Since spacecraft radio systems are optimized for telecommunications, certain drawbacks have hindered their utilization as radio-sounding beacons. For example, spacecraft radio communications were limited almost exclusively to the S band range ($\lambda \simeq 13$ cm) in the early years of interplanetary exploration. The prerequisite of having two widely separated carrier frequencies for performing dispersion measurements was fulfilled only when it became advantageous from a systems point of view to equip spacecraft with dual-freqency radio links. The addition of channels in the X band range ($\lambda \simeq 3.6$ cm) was driven by the requirement to accommodate higher bitrates. Nevertheless, the S band link was retained to provide a relatively risk-free, redundant communications capability. Even the dual-frequency S/X band instrument is not ideal for performing group time-delay measurements in interplanetary space. The sensitivity could be improved considerably with radio links at lower frequencies (Croft 1978).

For these reasons, differential group time-delay measurements in the inner heliosphere were not performed until the *Viking* mission (Tyler et al. 1977; Muhleman & Anderson 1981), more than a decade after the initial work with *Pioneer 6*. Single-frequency ranging measurements, it should be added, were used to infer coronal plasma structure during the solar conjunctions of *Mariner 6* and *Mariner 7* (Muhleman, Esposito, & Anderson 1977), and *Helios 1* (Esposito, Edenhofer, & Lüneburg 1980). These experiments are much more difficult to interpret because the group time delay is subject to contributions from nondispersive effects. This can become critical at small solar elongations where, for example, the much larger general relativistic time delay must be taken into account (Anderson et al. 1975). Subsequent to the *Viking* experiment, two *Voyager 2* opportunities were exploited for coronal ranging observations in the 1980's (Anderson et al. 1987; Krisher et al. 1991).

The results presented here are restricted to the total coronal electron content as determined from dual-frequency ranging measurements. For completeness, the measurement technique and process of ranging data reduction is outlined in some detail in the next section. The *Ulysses* results and their comparison with past experiments are presented in the following three sections. The much more sensitive dual-frequency Doppler data from the *Ulysses* solar conjunction, which provide *relative* but not *absolute* values for the columnar electron density along the signal ray path, are presently being processed and will be compared with the ranging results in a subsequent publication. The Doppler data will be further analyzed in order to yield a measure of the strength and spectral index of coronal turbulence.

2. MEASUREMENT TECHNIQUE

The ranging data used in this analysis were recorded primarily at the 70 m stations of the NASA Deep Space Network (DSN), located at Goldstone (California), Canberra (Australia) and Madrid (Spain). Some additional ranging data were taken at the smaller (34 m) stations at the three DSN complexes in California, Australia and Spain.

The nominal SCE radio system configuration during conjunction was to transmit two downlinks at S Band and X band, both of which were phase coherent with the S band uplink. The ranging "observable," the group delay time, is determined by measuring the time between the transmission of a coded signal and the reception at the ground station after being relayed back to Earth by the spacecraft radio transponder (Kinman 1992). This time measurement includes the round trip light time of the signal in free space and a delay due to the decrease in group velocity for propagation through an ionized medium. This delay is frequency dependent (dispersive) and proportional to the columnar electron density N_T ("electron content") of the traversed region (Bird & Edenhofer 1990). Using two downlink frequencies in coherent mode (S band: 2293 MHz; X band: 8408 MHz; $f_x/f_s = 11/3$) the delay of the S band ranging code with respect to the X band ranging code is given by

$$\Delta\tau = \frac{40.31}{c}\left[\frac{1}{f_S^2} - \frac{1}{f_X^2}\right]N_T\,, \qquad (1)$$

where c is the speed of light and f_S and f_X are the S and X band frequencies, respectively. Upon introducing the constant numerical values in equation (1), the total electron content in "hexems" (1 hexem = 10^{16} m^{-2}) is determined by the simple relation:

$$N_T = 4.225\,\Delta\tau\,, \qquad (2)$$

when the differential delay time $\Delta\tau$ is given in nanoseconds.

The measurements must be corrected for frequency-dependent contributions to signal delay inherent to the ground station and the spacecraft. The ground station time delays consist of a correction called the "station bias" that depends on the radio system configuration as well as a general differential delay calibration for each DSN station called the "Z-correction."

The spacecraft delay depends on such parameters as onboard temperature and uplink signal level as well as the selected radio frequency (RF) system configuration. Various RF system configurations were possible, depending upon which of the two redundant receivers was locked onto the uplink signal and which of the two redundant transmitters was used to drive each downlink. The *Ulysses* RF system configuration, unchanged during the entire conjunction, operated with the uplink signal received by receiver two (Rx 2), the S band downlink from transmitter one (Tx 1), and the X band downlink from Tx 2 (R. García Pérez 1992, private communication). From prelaunch dual-frequency ranging tests it was determined that the differential spacecraft delay varied from 18 to 24 ns for this configuration (Dornier System Star test report IS-TR-DS-4116, dated 1985 August 7). The sensitivity of the differential spacecraft delay to temperature was determined from these same tests to be less than 0.1 ns K^{-1} for this RF system configuration over the specified range of operating temperatures. Receiver and transmitter temperatures in transponder one (Rx 1 and Tx 1) were found to be 30 ± 2 and 44 ± 2 C, respectively. These same values for Rx 2 and Tx 2 were 16 ± 1 and 18 ± 1 C, respectively. The scatter in the spacecraft differential range delay due to temperature variations is thus estimated to be less than 1 ns. The uplink signal level recorded on the *Ulysses* spacecraft was maintained within bounds between -128 and -118 dBm throughout the solar conjunction measurement interval (R. García Pérez 1992, private communication). Pre-launch tests revealed a weak linear increase in the differential delay (~ 5 ns) when the uplink signal power decreased over this range. Changes in the spacecraft differential delay attributed to fluctuations in uplink power are thus certainly no greater than 5 ns and probably less. At any rate, the variations in $\Delta\tau$ due to changes in temperature and uplink signal power are negligible compared with those due to the day-to-day variations in interplanetary electron content. As a consequence, it was considered sufficient to use a constant mean value of 20 ns for the spacecraft delay correction to all range measurements over the duration of the conjunction.

The station bias is regularly measured at all DSN stations. Since the receiver configuration at each station was left unchanged for the duration of the solar conjunction, this parameter is basically a constant for each ground station. The Z-correction could also be considered a constant for each specific DSN station. This parameter is updated after recalibrations that are typically performed semiannually or after major station hardware renovations affecting the signal path. All of these calibration parameters are provided to the users for each individual range measurement.

Table 1 lists typical correction values for the specific DSN ground stations. These should be compared with the magnitude of actually measured differential delays. The calibration is

TABLE 1

TYPICAL CORRECTION VALUES FOR *ULYSSES* RANGING OBSERVATIONS

DSN Tracking Station	Frequency Band	Ground Station Delay (ns)	Z-correction (ns)	Total Differential[a] Calibration (ns)
		70 m Stations		
DSS 14	S	11538	26	
	X	11299	15	
	S – X	239	11	270
DSS 43	S	11508	90	
	X	11424	42	
	S – X	84	48	152
DSS 63	S	12423	96	
	X	12358	72	
	S – X	65	24	109
		34 m Stations		
DSS 12	S	10432	−135	
	X	10373	−144	
	S – X	59	9	88
DSS 42	S	10813	−124	
	X	10626	−102	
	S – X	187	−22	185
DSS 61	S	10770	−127	
	X	10643	−135	
	S – X	127	8	155

[a] Includes a constant differential delay time in the spacecraft radio system of 20 ns.

extremely important at the solar offset distance of 100 $R_\odot$, where the uncorrected value is $\Delta\tau \simeq 350$ ns (calibration correction: 80%), and can practically be neglected at small solar elongations. At $R = 8\ R_\odot$, for example, the uncorrected group delay time reaches $\Delta\tau \simeq 6650$ ns (calibration correction: 2%).

3. OBSERVATIONS

Figure 1 shows a solar disk view of the occultation geometry in a solar equatorial coordinate system. The ray path from *Ulysses* to Earth, moving from the solar east limb to the west limb at an average speed of 2.65 $R_\odot$ day^{-1}, reached its solar proximate distance of 4.3 $R_\odot$ on 1991 August 21.0. The small circles along the *Ulysses* trajectory indicate the spacecraft's position at 0 UT on each day. The signal passed through regions of heliolatitude greater than 45° only during three days around solar closest approach. The tips of the triangles in Figure 1 indicate the position along the trajectory at which good dual-frequency ranging measurements were recorded (one triangle for each DSN tracking pass). The tracking coverage of the *Ulysses* solar conjuction for ray paths inside of 40 $R_\odot$ was generally superior to that for the previous experiments with *Viking* or *Voyager*. This was accomplished even though the received signal level was degraded by the necessity to point the *Ulysses* downlinks away from the Earth for 14 days about conjunction in order to maintain spacecraft maneuverability. The maximum off-pointing of 1°.6, which occurred exactly at C_1, resulted in a 15 dB loss to the X band signal strength. Although the telemetry rate had to be dropped to its absolute minimum and the ranging data became very noisy during a few days near C_1, both S and X band carrier signals were kept in lock throughout the solar occultation.

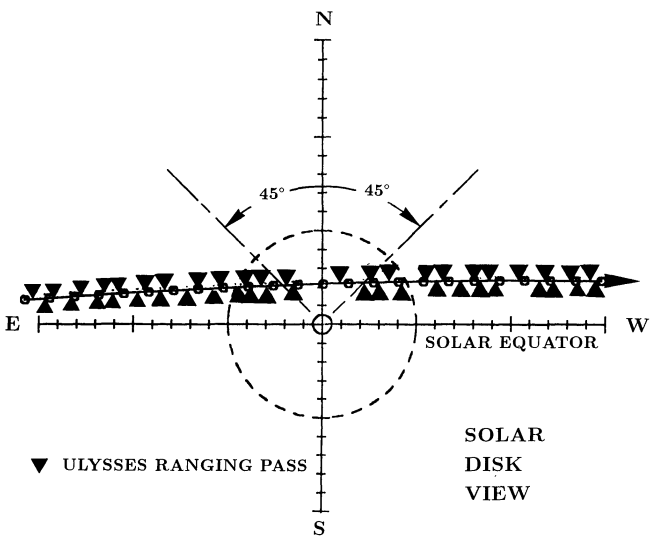

FIG. 1.—Solar disk view of *Ulysses* occultation geometry in 1991 August. This solar equatorial projection shows the apparent position of *Ulysses* as it passes behind the Sun from east to west solar limb at about 2.65 $R_\odot$ days^{-1}. The dashed circle centered on the Sun has a radius of 10 $R_\odot$. Dual-frequency ranging measurements were taken at the points along the trajectory indicated by the tips of the triangles. Only three tracking passes were recorded for which the ray path passed through heliolatitudes above 45°.

One advantage of the SCE measurement technique is that the signal ray path executes a fairly swift radial scan of the interplanetary plasma distribution. A global picture of coronal structure can thus be assembled over a period of only about one mouth. This time scale, unfortunately, also happens to be close to the solar rotation period. As a result, the east solar limb configuration scanned during occultation ingress rotates around to become essentially the west limb configuration scanned during occultation egress.

Figure 2 presents the total electron content inferred from the *Ulysses* ranging measurements during C_1 as a function of time. Each point represents the mean differetial range determined over a given tracking pass. A total of 30–50 individual range determinations were typically performed during each pass for

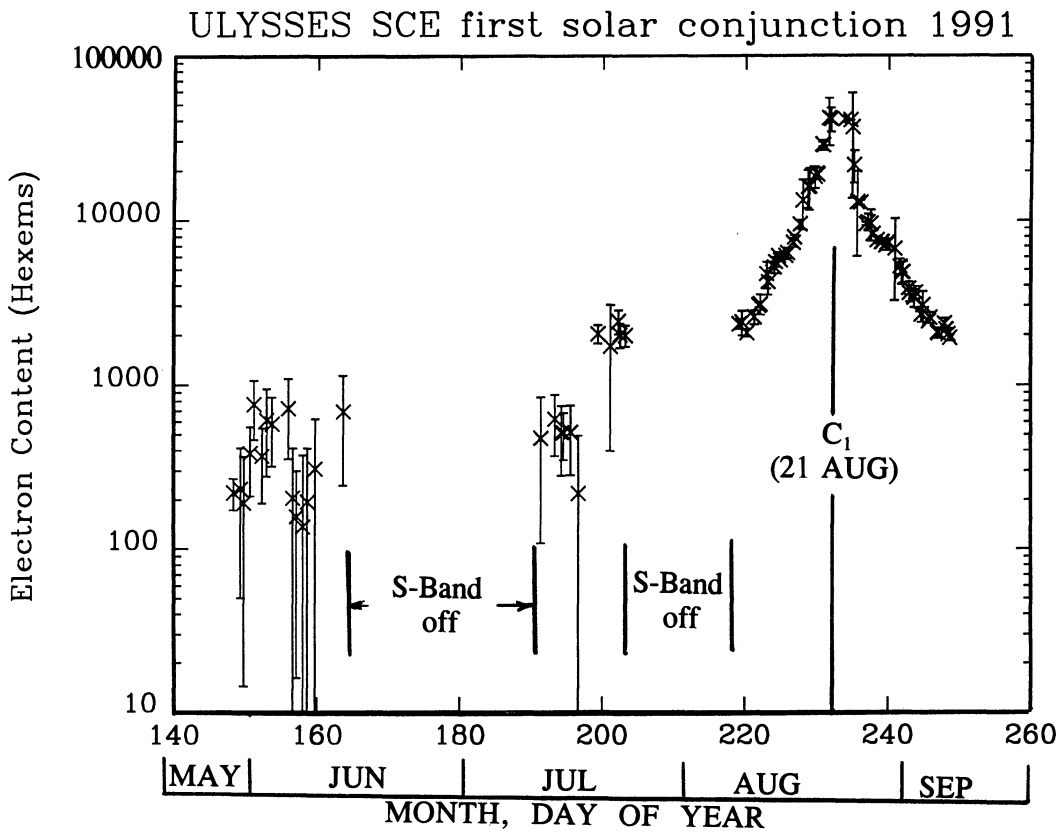

FIG. 2.—Mean total electron content versus observation date. Dual-frequency ranging measurements began on 1991 May 28 ($R \simeq 180\ R_\odot$). The S band downlink was switched off due to power restraints from June 14 to July 9 and from July 23 to August 5, respectively. From August 6 ($36 R_\odot$ east limb) to September 5 ($42 R_\odot$ west limb) almost continuous coverage was provided by the DSN ground stations. The closest approach of the ray path to the north pole of the Sun was $R = 4.3 R_\odot$, occurring at the conjunction epoch 1991 August 21.0.

the nominal ranging integration time of 10 minutes. The error bars indicate the rms variation about the mean value for each pass. The SCE measurements began on 1991 May 28 at east solar elongation $\epsilon \simeq 56°$, corresponding to a solar offset distance of $R \simeq 180\ R_\odot$. Two conspicuous data gaps are apparent in Figure 2. Due to power problems on-board *Ulysses* it was decided to switch off the S band downlink from June 14 to July 9 ($154\ R_\odot > R > 104\ R_\odot$) and again from July 23 to August 5 ($73\ R_\odot > R > 38\ R_\odot$). The resulting data gaps of four and two weeks, respectively, significantly depreciated the coverage of the ingress phase of the solar occultation. The dual-frequency SCE measurements were terminated on 1991 September 5, much earlier than originally planned, when the S band downlink was switched off again in order to save power for the on-board tape recorders. Since good measurements were only available for the time period ± 14 days about conjunction, detailed analysis of the data was restricted to two time segments: (A) the ingress phase on the east solar limb, starting from $36\ R_\odot$ down to the closest approach point of $4.3\ R_\odot$ (1991 August 21.0) and (B) the egress phase on the west solar limb from $4.3\ R_\odot$ out to $42\ R_\odot$. Table 2A (ingress) and Table 2B (egress) list the mean values of $\Delta\tau$ and N_T and their standard deviations ($1\ \sigma$) for each tracking pass in these two intervals.

4. ELECTRON DENSITY DISTRIBUTION

The total electron content is the integral of the electron density along the ray path from the spacecraft to the ground

TABLE 2A

ULYSSES DUAL-FREQUENCY RANGING MEASUREMENTS DURING SOLAR CONJUNCTION C_1: INGRESS PHASE

TIME (DOY)[a]	DSS	R ($R_\odot$)	θ	$\Delta\tau$ (ns)	$\pm\sigma_{\Delta\tau}$ (ns)	N_T (hexem)	$\pm\sigma_{N_T}$ (hexem)
220.21.....	43	33.0	7°.5	489.6	9.2	2056.3	38.6
221.26.....	43	30.3	8.2	607.6	19.0	2551.9	79.8
221.88.....	14	28.7	8.6	717.2	7.8	3012.2	32.8
222.10.....	43	28.1	8.8	730.2	33.5	3066.8	140.7
222.94.....	14	26.2	9.4	1119.4	70.6	4701.5	296.5
223.16.....	43	25.7	9.6	1000.4	56.3	4201.7	236.5
223.98.....	14	23.6	10.5	1235.4	34.5	5188.7	144.9
224.16.....	43	23.1	10.7	1331.9	31.6	5594.0	132.7
224.60.....	63	21.9	11.3	1451.3	24.8	6095.5	104.2
224.83.....	14	21.4	11.6	1366.8	7.3	5740.6	30.7
225.60.....	63	19.3	12.8	1457.1	27.0	6119.8	113.8
225.86.....	14	18.7	13.3	1514.1	35.3	6359.2	148.3
226.66.....	63	16.8	14.8	1747.3	38.5	7338.7	161.7
226.80.....	14	16.5	15.1	1886.7	18.0	7924.1	76.9
227.60.....	63	14.5	17.3	2257.8	46.2	9482.8	194.0
228.00.....	43	13.5	18.6	3147.8	352.2	13220.8	1479.2
228.68.....	63	11.7	21.6	3806.3	331.5	15986.5	1392.3
228.90.....	14	11.1	22.8	3828.0	362.0	16077.6	1522.1
229.67.....	63	9.3	27.4	4370.1	218.1	18354.4	916.0
229.90.....	14	8.8	29.2	4590.3	117.0	19279.3	494.3
230.04.....	43	8.5	30.3	4505.3	75.9	18922.3	318.8
230.65.....	63	7.4	35.6	6874.4	65.4	28872.5	274.7
230.80.....	14	7.1	37.2	6795.1	157.1	28539.4	659.8
231.60.....	63	5.6	50.0	9921.6	1058.1	41670.7	4444.0
231.86.....	14	5.1	57.1	9806.3	550.7	41186.5	2312.9

[a] Day of year.

TABLE 2B

Ulysses Dual-Frequency Ranging Measurements During Solar Conjunction C_1: Egress Phase

Time (DOY)[a]	DSS	R ($R_\odot$)	θ	$\Delta\tau$ (ns)	$\pm\sigma_{\Delta\tau}$ (ns)	N_T (hexem)	$\pm\sigma_{N_T}$ (hexem)
233.80.....	14	5.1	57°7	9804.5	157.8	41178.9	662.8
234.62.....	63	6.4	42.3	9660.0	0.0	40572.0	0.0
234.88.....	14	6.9	38.7	8747.4	1827.3	36739.1	7674.7
235.13.....	43	7.4	35.5	5172.4	381.8	21724.1	1603.6
235.61.....	63	8.5	30.5	3090.7	551.7	12980.9	2317.1
236.08.....	43	9.5	26.9	3059.0	36.6	12847.8	153.7
236.84.....	14	10.9	23.2	2272.1	18.1	9542.8	76.0
237.12.....	43	11.6	21.8	2327.6	93.1	9775.9	391.0
237.51.....	63	12.7	19.7	2277.5	163.2	9565.5	685.4
237.82.....	14	13.7	18.3	1976.0	21.4	8299.2	89.9
238.41.....	63	15.1	16.5	1805.0	30.2	7581.0	126.8
239.00.....	14	16.4	15.2	1761.0	15.8	7396.2	66.4
239.12.....	43	16.8	14.9	1760.4	22.7	7393.7	95.3
239.63.....	63	18.1	13.8	1682.1	41.4	7064.8	173.9
239.78.....	14	18.5	13.5	1744.3	31.9	7326.1	134.0
240.90.....	14	21.4	11.6	1604.5	280.1	6738.9	1176.4
241.65.....	63	23.3	10.6	1247.4	45.9	5239.1	192.8
241.88.....	12	23.9	10.3	1144.6	60.8	4807.3	255.4
242.07.....	43	24.4	10.1	1151.3	59.3	4835.5	249.1
242.88.....	14	26.5	9.3	910.4	26.2	3823.7	110.0
243.03.....	43	26.9	9.2	859.0	35.6	3607.8	149.5
243.64.....	63	28.5	8.7	794.5	34.1	3336.9	143.2
243.73.....	14	28.7	8.6	845.1	0.0	3549.4	0.0
245.74.....	63	34.0	7.3	571.9	6.2	2402.0	26.0
245.88.....	14	34.3	7.2	607.2	14.1	2550.2	59.2
246.92.....	14	37.1	6.7	488.2	10.5	2050.4	44.1
247.05.....	43	37.4	6.6	487.5	11.6	2045.4	48.7
247.90.....	14	39.7	6.2	554.1	14.4	2327.2	60.5
248.11.....	43	40.2	6.1	513.5	4.6	2156.7	19.3
248.42.....	61	41.1	6.0	481.2	12.8	2021.0	53.8
248.68.....	14	41.7	5.9	457.1	6.3	1919.8	26.5

[a] Day of year.

station:

$$N_T(R, \theta) = \int_{Ulysses}^{Earth} N(r)ds \,, \tag{3}$$

where R is the proximate distance of the signal ray path from the Sun (the "solar offset"), and $N(r)$ is the electron density at the position r along the ray path ds.

A modified Allen-Baumbach formula is commonly used to describe the electron density as a function of solar distance r and heliolatitude θ (Allen 1947; Tyler et al. 1977; Muhlman & Anderson 1981):

$$N(r, \theta) = \left[N_A \left(\frac{R_\odot}{r}\right)^6 + N_B \left(\frac{R_\odot}{r}\right)^\alpha \right] F(\theta) \,. \tag{4}$$

Sometimes a term in r^{-16} is included in this expression. However, this term and the first radial term in equation (4) are significant only for $r < 4\ R_\odot$, a region not probed by the *Ulysses* ray path to Earth. Various forms have been invoked for the latitudinal factor $F(\theta)$. In the case of the *Ulysses* conjunction, only three points in Figure 2 were recorded for which the heliolatitude at a ray path proximate point was greater than 45°. The electron density can thus be reliably expressed only by a single-power-law dependence using the last radial term in equation (4), with $\alpha \simeq 2$ if the solar wind expansion velocity is constant and radially symmetric. Introducing equation (4) into equation (3) and using the simple relations

$$s = R \tan \phi \Rightarrow ds = R \sec^2 \phi \, d\phi \,, \tag{5}$$

the total electron content for solar elongations near conjunction may be written to a good approximation as

$$N_T(R) = K(\alpha) N_B R_\odot \left[\frac{R_\odot}{R}\right]^{\alpha - 1} , \tag{6}$$

where

$$K(\alpha) = \int_{-\pi/2}^{\pi/2} \cos^{\alpha - 2} \phi \, d\phi = \sqrt{\pi} \left[\Gamma\left(\frac{\alpha - 1}{2}\right) \Big/ \Gamma\left(\frac{\alpha}{2}\right) \right] . \tag{7}$$

Using the single power-law model (6), mean values for α and N_B and their standard deviations were derived from the electron content measurements during both the ingress and egress phases. Linear power-law regression curves, fit to the data separately for ingress and egress, are shown in Figures 3*a* and 3*b*. The total electron content follows a single-exponent radial dependence with $\alpha = 2.54$ and $\alpha = 2.42$ during ingress and egress phase, respectively. The difference in overall electron density level between the east and west solar limbs, as indicated by the derived electron density at the nominal solar distance $r = 20\ R_\odot$, was only $\sim 10\%$.

The radial profile of electron density is intimately connected to the solar wind's radial velocity profile by the conservation of mass equation. The extensive in situ solar wind observations of the *Helios* spacecraft indicate that high-speed streams, emanating from large coronal holes, exhibit both smaller relative acceleration and smaller relative decrease in density between 0.3 to 1.0 AU than denser regions of slow solar wind (Schwenn 1990). If the solar with expansion is spherically symmetric in the range of solar distances applicable to those measurements ($r > 5\ R_\odot$), the steeper decrease in the density from the simple r^{-2} law implies significant solar wind acceleration out beyond at least 40 $R_\odot$. This conclusion, it should be emphasized, is subject to the validity of the assumption concerning spherical symmetry. When latitudinal and longitudinal variations are present (evidence for their existence, in fact, it demonstrated below), they can have a significant effect on the value of the falloff exponent α derived from radio occultation experiments of this type.

Four features are marked in each of the curves of Figure 3. These can be associated with large-scale latitudinal/longitudinal variations in the inner heliosphere. Discussion of these features is facilitated with the help of Figure 4, a contour map of the source surface magnetic field strength applicable for the time of the conjunction C_1 (kindly provided by J. T. Hoeksema 1993, private communication, as adapted from Solar-Geophysical Data). Selected signal ray paths from *Ulysses* to Earth are projected onto the same spherical surface of radius 2.5 $R_\odot$. Figure 4 extends $\pm 70°$ in heliographic latitude and 360° in heliospheric longitude, covering the last half of Carrington Rotation (CR) 1845 and the first half of CR 1846. Light shading represents positive magnetic polarity (away from the Sun), while dark shading denotes negative (toward) polarity. These regions are separated by a thick wavy line where the magnetic field vanishes, the trace of the heliospheric current (or neutral) sheet. Source surface maps of this type are known to reflect the same basic topology as the coronal electron density distribution (e.g., Bird & Edenhofer 1990). Further details concerning these maps are given in Hoeksema & Scherrer (1986).

The projection of the solar proximate point along the signal ray path for the ingress phase of the occultation is denoted by an "X" symbol. Points are plotted for 0 UT for each of the

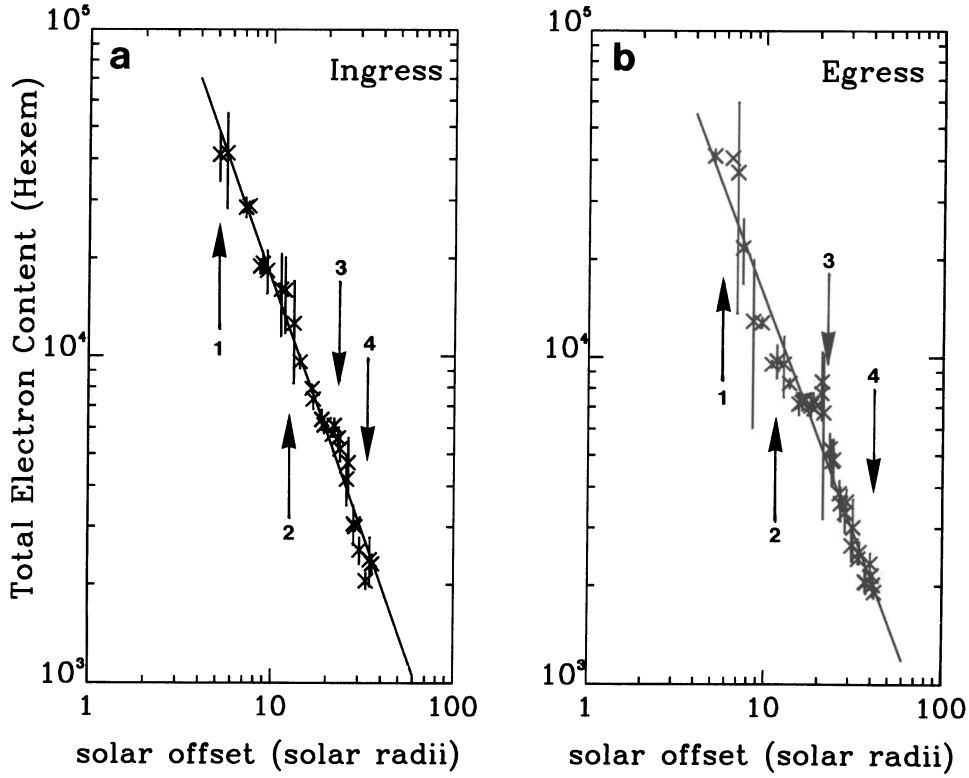

FIG. 3.—Total electron content N_T vs. solar offset distance R between 4 and 40 $R_\odot$. Radial power-law regression fits to the data were made for (*a*) ingress, and (*b*) egress. The error bars correspond to rms variation ($\pm 1\ \sigma$) over each tracking pass. The four numbered features in each curve are discussed in the text.

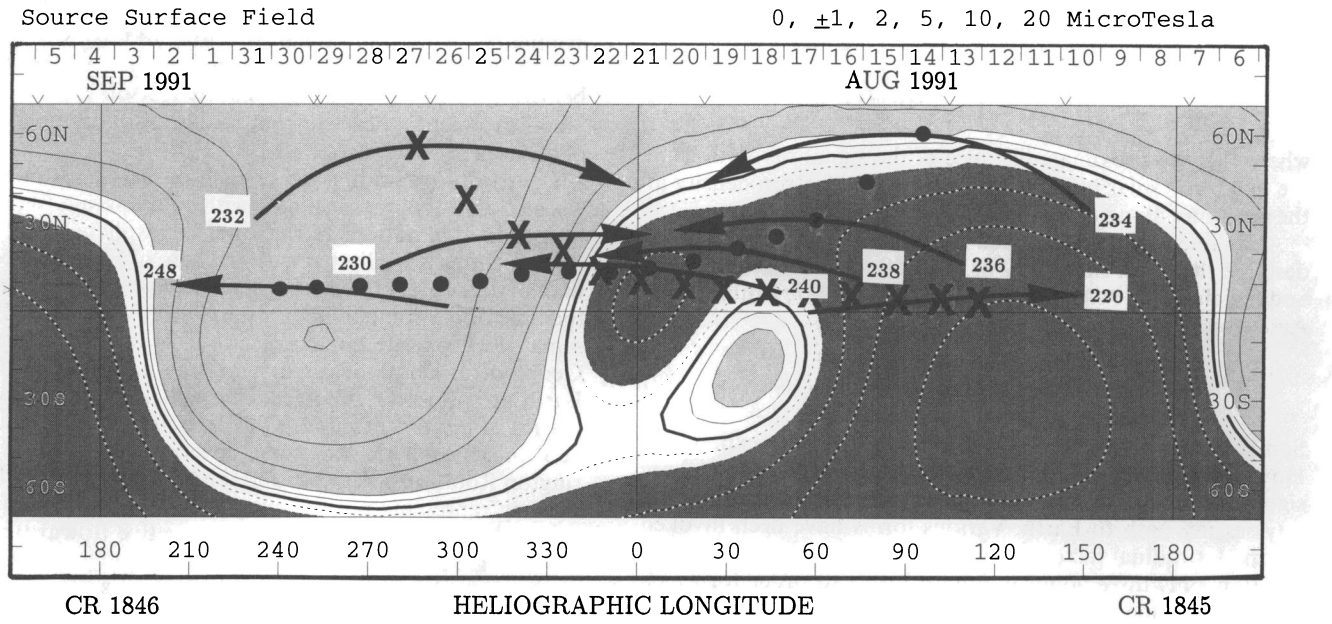

FIG. 4.—Projections of *Ulysses*/Earth ray paths onto a contour map of coronal magnetic field strength at 2.5 $R_\odot$. The contour map shows 360° of heliolongitudes with equal portions from Carrington rotations 1845 and 1846. The magnetic field polarity is predominantly positive (away, *light shading*) at northern heliographic latitudes and negative (toward, *dark shading*) in the south. The heliospheric current sheet, the separatrix between magnetic fields of opposite polarity, is tilted by about 60°with respect to the heliographic equator. The heliographic latitude and longitude of the *Ulysses* ray path's solar proximate point is shown at 0 UT for 14 days of occultation ingress ("X") and 16 days of occultation egress ("●"). Actual ray path segments near the solar proximate points (denoted by their 1991 days of year) are plotted for 3 ingress days and 5 egress days. Relatively low, or relatively high electron content is recorded, depending upon whether the ray path projects onto a monopolar region (coronal hole), or onto the heliographic current sheet (coronal streamer), respectively. The specially prepared contour map was provided by J. T. Hoeksema, Stanford University.

1991 days of year (DOY) 219–232 (1991 August 7–20). The corresponding points for the egress phase (DOY 234–249, 1991 August 22–September 6) are indicated by the filled circles. The ray path segments nearest the Sun, i.e., within $\pm 45°$ solar centered angular separation from the solar proximate point, are projected onto the map of Figure 4 for 3 days during ingress and 5 days during egress (marked with DOY numbers). Note in Figure 4 that, as mentioned earlier, the range of heliographic longitudes probed during conjunction egress overlapped considerably with that during the ingress phase.

Ray paths that lie wholly within large monopolar regions, usually associated with lower density coronal holes, would be expected to yield relatively lower electron contents. Ray paths crossing the neutral line, especially those running more or less parallel along the heliospheric current sheet, would generally produce higher electron contents. The numbered features of Figure 3 may now be correlated with the inferred nonradial variations in the electron density of the inner heliosphere. The location of the ray path from Figure 4 and the subsequent prediction for the measured electron content for each feature, centered approximately at the given 1991 DOY number and solar offset distance, is as follows.

Ingress.—1. DOY 232, $R \simeq 6\ R_\odot$: Ray path mostly in large (away) monopolar sector ($\Rightarrow$low N_T).

2. DOY 228, $R \simeq 13\ R_\odot$: Ray path crosses heliospheric current sheet (coronal streamer) near solar proximate point ($\Rightarrow$high N_T).

3. DOY 224, $R \simeq 23\ R_\odot$: Ray path passes through isolated lobe of magnetic neutral sheet ($\Rightarrow$high N_T).

4. DOY 221, $R \simeq 31\ R_\odot$: Ray path mostly in large (toward) molopolar sector ($\Rightarrow$low N_T).

Egress.—1. DOY 234, $R \simeq 6\ R_\odot$: Ray path runs almost parallel along heliospheric current sheet ($\Rightarrow$very high N_T).

2. DOY 237, $R \simeq 11\ R_\odot$: Ray path mostly in large (toward) monopolar sector ($\Rightarrow$low N_T).

3. DOY 241, $R \simeq 22\ R_\odot$: Ray path crosses heliospheric current sheet near solar proximate point ($\Rightarrow$high N_T).

4. DOY 248, $R \simeq 40\ R_\odot$: Ray path mostly in large (away) monopolar sector ($\Rightarrow$low N_T).

The nonradial variations inferred from the comparison with Figure 4 were significant perturbations to the observed radial profiles $N_T(R)$, but more or less compensated each other in the final least-square determination of the electron density level N_B and radial falloff exponent α for both ingress and egress. This need not have been the case for the previous dual-frequency radio-sounding experiments with *Viking* and *Voyager*. Dependuing on just when coronal streamers and/or holes happened to rotate into the signal ray path, one could easily obtain significant distortions in the radial profile of coronal electron content.

5. COMPARISON WITH PREVIOUS RADIO OCCULTATION EXPERIMENTS

The electron density radial profile parameters using the second term of equation (4) derived for the *Ulysses* solar conjunction are compared in Table 3 with similarly derived parameters from the earlier experiments on *Voyager 2*. In order to guarantee a consistent comparison, the data in Table 3 were all generated using the same unweighted least-squares fitting procedure. The rederived *Voyager* parameters agree with the previously published values (Anderson et al. 1987; Krisher et al. 1991) to within the formal standard errors of the regression analysis. As indicated above, no fit was attempted

TABLE 3

ELECTRON DENSITY RADIAL PROFILE PARAMETERS: $N(R) = N_B(R_\odot/R)^\alpha$

Parameter	Ingress	Egress
Ulysses—1991 August: Solar Maximum + 25 Months		
Total range measurements	25	31
Range of validity ($R_\odot$)	5–33	5–42
Radial falloff exponent α.....	2.54 ± 0.05	2.42 ± 0.05
N_B(cm^{-3})	$3.61 \pm 0.04 \times 10^6$	$2.26 \pm 0.03 \times 10^6$
$N(20\ R_\odot)$(cm^{-3})	$1.8 \pm 0.1 \times 10^3$	$1.6 \pm 0.1 \times 10^3$
Voyager—1988 December: Solar Maximum − 7 Months		
Total range measurements	9	12
Range of validity ($R_\odot$)	10–85	14–88
Radial falloff exponent α.....	2.08 ± 0.05	2.28 ± 0.05
N_B(cm^{-3})	$2.95 \pm 0.04 \times 10^6$	$6.94 \pm 0.11 \times 10^6$
$N(20\ R_\odot)$(cm^{-3})	$5.8 \pm 0.4 \times 10^3$	$7.5 \pm 0.5 \times 10^3$
Voyager—1985 December: Solar Minimum − 9 Months		
Total range measurements	7	7
Range of validity ($R_\odot$)	6–38	7–38
Radial falloff exponent α.....	2.63 ± 0.07	1.94 ± 0.07
N_B(cm^{-3})	$4.13 \pm 0.07 \times 10^6$	$0.52 \pm 0.01 \times 10^6$
$N(20\ R_\odot)$(cm^{-3})	$1.6 \pm 0.2 \times 10^3$	$1.5 \pm 0.1 \times 10^3$

for possible latitudinal variations due to the paucity of *Ulysses* data above 45° heliolatitude.

The same problem was evident during the solar occultations of the *Voyager 2* spacecraft in 1985 December and 1988 December, respectively. A total of 14 dual-frequency ranging passes were performed in 1985 December, an epoch of minimum solar activity ($R_Z = 15$), between 6 and 40 $R_\odot$. The coronal electron content given by equation (6) was found to be asymmetric, significantly different parameters being necessary for the ingress and egress phases of the occultation (Anderson et al. 1987). During solar maximum conditions in 1988 December Krisher et al. (1991) derived a more symmetric coronal structure, but with an exceptionally high electron density level. In this special case the model parameters given in Table 3 are restricted to $r > 10\ R_\odot$. Inside this distance the electron density tended to increase more rapidly ($\alpha \simeq 2.7 \pm 0.2$), perhaps an indicator of a heliolatitude effect. The two ranging measurements taken closest to the Sun in 1988 December, which deviated greatly from the regression curve, were excluded.

Viking dual-frequency ranging measurements performed during solar minimum conditions in 1976 (Muhleman & Anderson 1981) were used to derive the following best-fit model for the electron density at this epoch:

$$N(r, \theta) = 1.32 \times 10^6 \left(\frac{R_\odot}{r}\right)^{2.7} \exp\left[-\left(\frac{\theta}{8}\right)^2\right] + 0.23 \times 10^6 \left(\frac{R_\odot}{r}\right)^{2.04}. \quad (8)$$

The *Viking* solar occultation geometry, together with the extensive database resulting from the excellent tracking coverage, enabled Muhleman & Anderson (1981) to adopt two radial terms in equation (8), the first of which is dependent on heliographic latitude θ. These two terms are equal in the solar

equator at $r \simeq 14\ R_\odot$. The radial decrease for solar distances greater than 60 $R_\odot$ is governed by the second term of equation (8) with $\alpha = 2.04 \pm 0.02$. This is consistent with the radial falloff $\alpha = 2.10 \pm 0.04$ determined by the plasma detector on board *Helios* during the same time period (Bougeret, King, & Schwenn 1984). The equatorial electron density from equation (8) at $r = 20\ R_\odot$ is 915 cm^{-3}. As may be seen from Table 3, this density is lower than that determined at all subsequent dual-frequency ranging experiments.

The electron density profiles obtained from the *Ulysses* coronal ranging observations are shown together with the rederived *Voyager* profiles and the solar minimum electron density profile inferred from *Viking* observations in 1976 in Figure 5. Each curve in Figure 5 is restricted to that range of solar distances over which the measurements were used in the linear regression analysis.

The *Ulysses* profiles for ingress and egress lie very close to, but are not nearly as asymmetric as, the *Voyager* 1985 profiles. The electron density level derived from the *Voyager* 1988 data, as noted by the authors, appears to have been exceptionally high. Considering that it was more than two years after the acknowledged maximum of solar cycle 22, the *Ulysses* ranging observations in 1991 August were recorded during a period of remarkably high solar activity. Even though the mean smoothed sunspot number in 1991 August was $R_Z = 146$, the mean *Ulysses* coronal density at 20 $R_\odot$, weighted over both solar limbs, was $1.7 \pm 0.1 \times 10^3$ cm^{-3}. This is nearly a factor of 4 lower than the corresponding value of $N(20\ R_\odot) = 6.5 \pm 0.3 \times 10^3$ cm^{-3} for *Voyager* in 1988 December ($R_Z = 138$).

An analysis of the 1988 December source surface maps published in Solar Geophysical Data revealed that the inferred coronal electron density distribution in heliographic longitude and latitude was surprisingly similar to that in 1991 August. The polarities of the solar polar regions were reversed, but the tilt of the heliospheric current sheet was again $\simeq 60°$. Noting the effects of the *Ulysses* electron content profiles discussed in the previous section, it was suspected that the unusually high level of electron density observed during the *Voyager* conjunction in 1988 might be attributed to the fact that the signal ray path was oriented almost continuously along a coronal streamer. With the exception of the two outermost ranging points, a coronal streamer, rather than a coronal hole, was located on the solar east limb (probed by the *Voyager* downlink during the ingress phase). The situation for the egress phase was less convincing. Of the 12 ranging points used in the least-squares fitting analysis, eight were recorded when the heliospheric current sheet was near the west solar limb. The ray paths associated with the remaining four points were oriented essentially parallel to, albeit between 15°–30° north of, the heliospheric current sheet, at least in the projection onto the source surface at 2.5 $R_\odot$. It is conceivable, but very speculative, that the heliospheric current sheet would curve toward lower latitudes and intersect the signal ray path at the larger solar offset distances (30–50 $R_\odot$) where these measurements were taken.

The empirical model (8) for the *Viking* measurements in 1976 is practically indistinguishable from a straight line (single-power law). For comparison with the other entries in Table 3, suitable values of the electron density model parameters for the

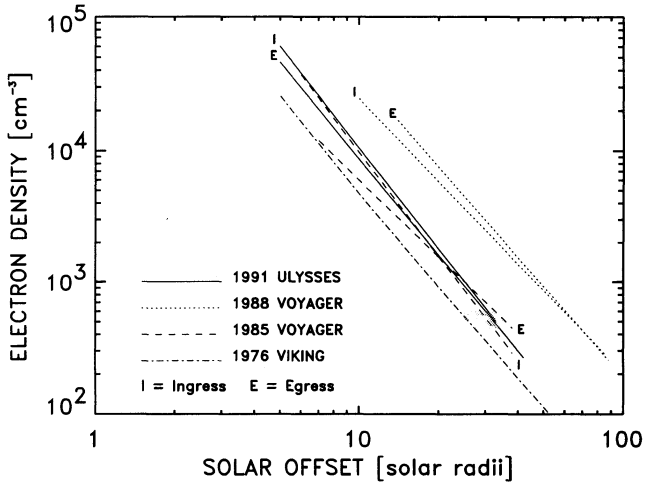

FIG. 5.—Comparison of radial electron density profiles obtained at various phases of the solar cycle. Two-frequency ranging measurements were obtained during the following solar occultation experiments: *Ulysses* 1991 August (*solid lines*), *Voyager* 1988 December (*dotted lines*), *Voyager* 1985 December (*dashed lines*), *Viking* 1976 November (*dashed-dotted line*). The letters "I" and "E" denote ingress and egress, respectively. The curves are plotted only for the range of solar distances over which the measurements were taken.

Viking 1976 solar occultation are given by

$$N_B = 0.99 \times 10^6\ \text{cm}^{-3}\ \alpha = 2.32\ . \qquad (9)$$

The coronal symmetry implied by the data obtained during the *Ulysses* conjunction was not completely unexpected. Symmetric coronae are characteristic for the extended solar maximum conditions in 1991 August. In spite of this long-standing "tradition," the exceptional total solar eclipse of 1991 July 11 revealed a distinctly asymmetric corona with strong streamer development in the NE and SW quadrants (e.g., Zirker et al. 1992). It is conjectured that the coronal structure during the *Ulysses* conjunction C_1 was probably similar to that observed as a "snapshot" during the eclipse one month earlier. The month-long duration of the radio occultation experiment, combined with a more or less rigid solar rotation, was responsible for the apparent similarity of the ingress and egress observations.

The Solar Corona Experiment on *Ulysses* could not have been performed without many contributions from the Radio Science Support Team at the Jet Propulsion Laboratory. We especially appreciate the efforts of A. S. Devereaux, P. M. Eshe, R. G. Herrera, T. Horton, and D. D. Morabito. We also acknowledge the assistance of the *Ulysses* Spacecraft Operations Team, in particular N. Angold and R. García Pérez, who have responded promptly and conscientiously to the specialized requirements of this investigation. This paper presents results of a research project partially funded by the Deutsche Agentur für Raumfahrtangelegenheiten (DARA) GmbH under contract 50 ON 9104. The responsibility for the contents of this publication is assumed by the authors.

REFERENCES

Allen, C. W. 1987, MNRAS, 107, 426
Anderson, J. D., Esposito, P. B., Martin, W., & Thornton, C. L. 1975, ApJ, 200, 221
Anderson, J. D., et al. 1987, ApJ, 323, L141
Bird, M. K., & Edenhofer, P. 1990, in Physics of the Inner Heliosphere, ed. R. Schwenn & E. Marsch (Heidelberg: Springer), 13
Bird, M. K., Asmer, S. W., Brenkle, J. P., Edenhofer, P., Pätzold, M., & Volland, H. 1992, A&AS, 92, 425
Bougeret, J.-L., King, J. H., & Schwenn, R. 1984, Solar Phys., 90, 401
Croft, T. A. 1978, in A Close-Up of the Sun, ed. M. Neugebauer & R. W. Davies (JPL Publication 78-70), 397
Esposito, P. B., Edenhofer, P., & Lüneburg, E. 1980, J. Geophys. Res., 85, 3414
Eshleman, V. R., Garriott, O. K, Leadabrand, R. L., & Peterson, A. M. 1966, J. Geophys. Res., 71, 3325
Hoeksema, J. T., & Scherrer, P. H. 1986, The Solar Magnetic Field—1976 through 1985, (WDC-A Report UAG-94)
Kelso, J. M. 1959, J. Atm. Terr. Phys., 16, 357
Kinman, P. W. 1992, IEEE Trans. Microwave Theory Tech., 40, 1199
Krisher, T. P., et al. 1991, ApJ, 75, L57
Muhleman, D. O., & Anderson, J. D. 1981, ApJ, 247, 1093
Muhleman, D. O., Esposito, P. B., & Anderson, J. D. 1977, ApJ, 211, 943
Pätzold, M., Bird, M. K., Volland, H., Asmar, S. W., & Brenkle, J. P. 1992, in Solar Wind Seven, ed. E. Marsch & R. Schwenn (Oxford: Pergamon), 237
Schwenn, M. 1990, in Physics of the Inner Heliosphere, ed. R. Schwenn & E. Marsch (Heidelberg: Springer), 99
Tyler, G. L., Brenkle, J. P., Komarek, T. A., & Zygielbaum, A. I. 1977, J. Geophys. Res., 82, 4335
Zirker, J. B., et al. 1992, A&A, 258, L1